

PolarQuant: Leveraging Polar Transformation for Efficient Key Cache Quantization and Decoding Acceleration

Songhao Wu^{1*} Ang Lv^{1*}

Xiao Feng² Yufei Zhang³ Xun Zhang³

Guojun Yin^{3†} Wei Lin³ Rui Yan^{1†}

¹Renmin University of China ²ShanghaiTech University ³Meituan

{songhaowu, anglv, ruiyan}@ruc.edu.cn

fxiao369@gmail.com

{zhangyufei08, zhangxun12, yinguojun02, linwei31}@meituan.com

Abstract

The KV cache in large language models is a dominant factor in memory usage, limiting their broader applicability. Quantizing the cache to lower bit widths is an effective way to reduce computational costs; however, previous methods struggle with quantizing key vectors due to outliers, resulting in excessive overhead. We propose a novel quantization approach called PolarQuant, which efficiently addresses the outlier challenge. We observe that outliers typically appear in only one of two dimensions, which are rotated together by a specific angle when rotary position embeddings are applied. When represented as two-dimensional vectors, these dimensions exhibit well-structured patterns, with radii and angles smoothly distributed in polar coordinates. This alleviates the challenge of outliers on per-channel quantization, making them well-suited for quantization. Thus, PolarQuant divides key vectors into groups of two-dimensional sub-vectors, encoding them as the corresponding quantized radius and the polar angle, rather than quantizing original key vectors directly. PolarQuant achieves the superior efficiency in KV cache quantization and accelerates the decoding process by turning the query-key inner product into a table lookup, all while maintaining the downstream performance of full-precision models.

1 Introduction

Large language models (LLMs) have achieved remarkable success across a wide range of applications. As these models continue to advance, the demand for enhanced long-context capabilities also increases, encompassing tasks such as contextual retrieval in question answering (Liu et al., 2024) and long-context generation for deep reasoning and reflection (OpenAI, 2024). However, a significant

challenge in developing long-context LLMs is the rising memory cost associated with increasing context lengths, which hinders both their practical deployment and further research.

The attention mechanism (Bahdanau et al., 2016) in LLMs¹ is a major contributor to memory consumption, as its memory requirements typically grow quadratically with context length. To mitigate this overhead, a common strategy is to cache the key and value vectors (known as the KV cache) from previous contexts, thereby avoiding the need to recompute the entire quadratic attention weight matrix. Nonetheless, in long-context scenarios, the memory required for the KV cache often exceed that consumed by the LLM’s weights, making it the dominant factor in overall memory usage.

A series of solutions is proposed to reduce the memory cost associated with the KV cache. Some studies introduce memory-efficient attention modules, such as GQA (Ainslie et al., 2023) and MLA (DeepSeek-AI et al., 2024). While these methods show promise for training future LLMs from scratch, they cannot be applied to existing pre-trained LLMs, which limits their generalizability. Another research direction focuses on reducing the size of the KV cache in a manner compatible with existing LLMs. This includes techniques like KV cache eviction (Zhang et al., 2023; Li et al., 2024; Cai et al., 2024), which removes key and value vectors of unimportant tokens from the cache, and quantization (Liu et al., 2025; Hooper et al., 2024; Zhao et al., 2024; Kang et al., 2024), which represents cached key and value vectors in low bits.

This paper focuses on the cache quantization. In general, key and value vectors are quantized along different axes. Although value caches can be quantized on a token-wise basis (Liu et al., 2025)

¹In this paper, we focus on decoder-only Transformer-based (Vaswani et al., 2017) LLMs using rotary position embedding (RoPE, Su et al., 2023), which are the predominant implementation of advanced LLMs.

* Equal contribution.

† Corresponding authors.

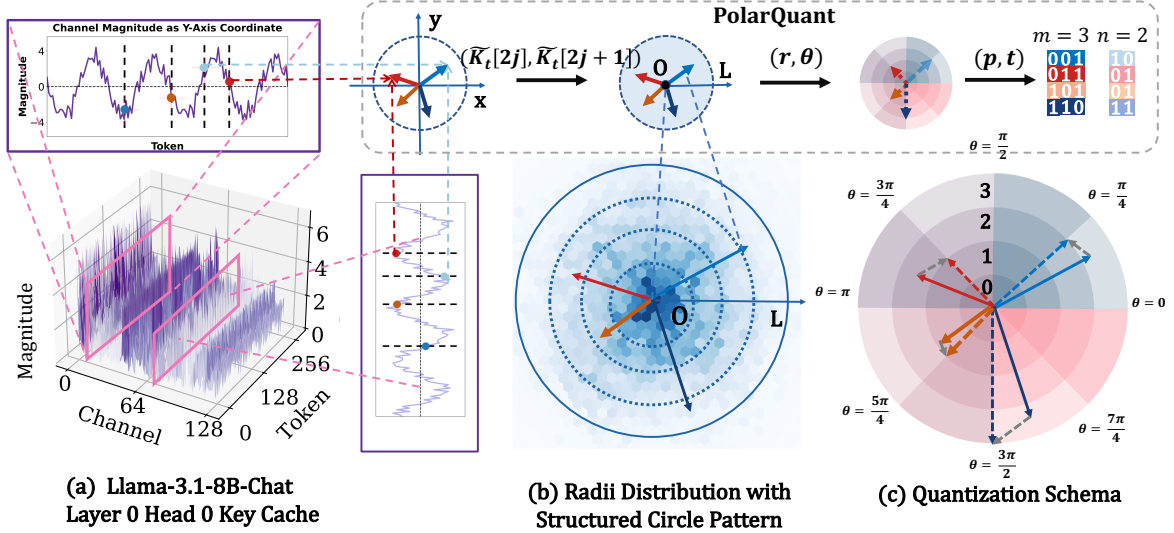


Figure 1: (a) Illustration of outliers in key vectors. We highlight two dimensions rotated together by RoPE that exhibit outliers (exemplified by Llama 3.1-8B-Instruct Layer 0 Head 0). (b) When viewing these two dimensions in a two-dimensional plane, although the individual x- or y-axis may contain outliers, they collectively form stable circular patterns, making quantization of the original outliers easier. Each blue dot represents a mapped two-dimensional vector, with transparency indicating frequency. (c) An example of PolarQuant using $m = 3$ bits to quantize polar angles and $n = 2$ bits to quantize radii. The colorful arrows indicate sub-vectors formed by pairs of dimensions in the keys; the quantized results are shown with colorful dashed arrows, and the quantization error is represented by the grey dashed arrow.

(i.e., across dimensions within each token position), quantizing the key cache is more challenging due to its channel-wise distributed outliers (Liu et al., 2025; Hooper et al., 2024), as shown in Figure 1(a) (i.e., some specific dimensions at each token position contain outliers). Liu et al. (2025) reveal channel-wise outliers, divide tokens into groups, and quantize tokens in each group along the specific dimension where outliers occur. Hooper et al. (2024) note that RoPE disrupts the magnitudes of outliers at certain token positions, and they proposed channel-wise quantization of key vectors before applying RoPE (pre-RoPE). However, these existing methods face a dilemma: quantizing post-RoPE keys demands fine-grained token grouping, whereas quantizing and caching pre-RoPE keys requires on-the-fly dequantization when applying RoPE—both of which result in overhead.

In this paper, we propose a new perspective on handling outliers in the key cache, effectively addressing the quantization dilemma. Recall that RoPE applies a rotation to every two-dimensional sub-vector of the key vector using orthogonal 2×2 rotary matrices. For readers unfamiliar with RoPE, please refer to Section 2. When analyzed

in 2D polar coordinates, these sub-vectors form well-defined circular patterns, as illustrated in Figure 1(b). By encoding each sub-vector as its corresponding radius r and polar angle θ , we can represent the entire key vector using all radii and angles. This perspective transformation effectively mitigates outliers, as both the radii and polar angles become smoothly distributed. Building on this, we propose a novel quantization method, PolarQuant, under the rotation perspective, which significantly simplifies the quantization of the key cache. PolarQuant reduces the problem of quantizing key vectors to asymmetrically quantizing r and θ into an n -bit and an m -bit integer. Intuitively, PolarQuant defines 2^{n+m} distinct regions based on 2^m angles and 2^n radii. Each sub-vector is then encoded by the index of the region it belongs to. Figure 1(c) illustrates PolarQuant for $m = 3$ and $n = 2$.

PolarQuant achieves superior quantization efficiency over previous methods for three primary reasons: (1) Unlike pre-RoPE quantization (Hooper et al., 2024), which requires on-the-fly dequantization when applying RoPE on memory-bounded GPUs, PolarQuant eliminates this overhead entirely. (2) Smoother distributions

of radii and angles facilitate downstream performance preservation, so PolarQuant does not require the token grouping used in previous post-RoPE quantization (Liu et al., 2025). (3) PolarQuant also requires fewer quantization parameters, not only because it does not use grouping, but also because it leverages the non-negativity of the radii to avoid storing zero-points.

Additionally, **PolarQuant enables a novel decoding acceleration method.** In the attention mechanism, it replaces the standard query-key multiplication with inner products between two-dimensional query sub-vectors and a quantized polar coordinate representation of key sub-vectors, which have finite and deterministic states. This transforms matrix multiplication to a table lookup, greatly speeding up attention computation. Although this approach can be applied to previous post-RoPE quantization methods, the increased number of quantization states from token grouping negates any overall efficiency gain.

We implement Triton (Tillet et al., 2019) kernels for PolarQuant and our new decoding acceleration method. With $n = 4$ bit, we achieve an up-to $1.27\times$ speedup of query-key multiplication on various open-source LLMs, while maintaining comparable downstream performance to previous competitive methods.

Our contributions are threefold: (1) introducing polar transformation for quantization for the first time and deriving PolarQuant, a novel and efficient post-RoPE quantization method; (2) reducing the number of quantization parameters, thereby lowering quantization costs; and (3) proposing a new decoding acceleration algorithm as a natural byproduct of PolarQuant. We are committed to open source.

2 Background

Consider a specific Transformer layer where the input hidden states to the attention block are denoted as $\mathbf{X} \in \mathbb{R}^{T \times D}$, where T is the sequence length and D is the hidden state dimension. For an arbitrary attention head, the d -dimensional query, key, and value vectors are obtained by applying three linear transformations to \mathbf{X} . Specifically, for each head h , the corresponding computations are as follows:

$$\mathbf{Q} = \mathbf{X}\mathbf{W}_Q, \quad \mathbf{K} = \mathbf{X}\mathbf{W}_K, \quad \mathbf{V} = \mathbf{X}\mathbf{W}_V,$$

where each $\mathbf{W}_* \in \mathbb{R}^{D \times d}$, and the resulting variables have shapes of $\mathbb{R}^{T \times d}$.

The query and key vectors are then applied with RoPE (Su et al., 2023) to incorporate positional information. For a query or key vector at position $t \in [1, T]$, the corresponding rotary matrix $\mathbf{R}_{t,\Phi} \in \mathbb{R}^{d \times d}$ is defined as:

$$\mathbf{R}_{t,\Phi} = \begin{bmatrix} \mathbf{r}_{t,\phi_1} & \mathbf{O} & \cdots & \mathbf{O} \\ \mathbf{O} & \mathbf{r}_{t,\phi_2} & \cdots & \mathbf{O} \\ \mathbf{O} & \mathbf{O} & \cdots & \mathbf{r}_{t,\phi_{d/2}} \end{bmatrix} \quad (1)$$

where \mathbf{O} is a zero matrix, and each \mathbf{r}_{t,ϕ_i} for $i \in [1, \frac{d}{2}]$ is a 2×2 orthogonal matrix:

$$\mathbf{r}_{t,\phi_i} = \begin{bmatrix} \cos(t\phi_i) & -\sin(t\phi_i) \\ \sin(t\phi_i) & \cos(t\phi_i) \end{bmatrix}$$

Here, ϕ_i is typically defined as $\phi_i = b^{-2(i-1)/d}$, where b is a hyperparameter. This formulation encodes the relative distance $l - t$ between a query at position $l > t$ and a key at position t into their inner product, as shown by:

$$(\mathbf{Q}_l \mathbf{R}_{l,\Phi})(\mathbf{K}_t \mathbf{R}_{t,\Phi})^\top = \mathbf{Q}_l \mathbf{R}_{l-t,\Phi} \mathbf{K}_t^\top$$

In causal language models, such as generative LLMs, each token can only attend to preceding tokens. Therefore, the keys (after applying RoPE) and values of previous tokens—specifically $\mathbf{K}_t \mathbf{R}_{t,\Phi}$ (which we abbreviate as $\tilde{\mathbf{K}}_t$) and \mathbf{V}_t —are unaffected by future tokens. These vectors are thus cached, known as the KV cache, to avoid redundant recomputation. However, the size of the KV cache in large language models can become prohibitively large, often exceeding the number of model parameters. This presents a significant challenge when processing long contexts, making it essential to quantize the KV cache for more broader usage.

A value vector $\mathbf{V}_t \in \mathbb{R}^d$ is typically b -bit quantized per-token-wise, denoted as $Q(\mathbf{V}_t)$. For an arbitrary dimension $j \leq d$, we have:

$$Q(\mathbf{V}_t[j]) = \text{Clamp} \left(\left\lfloor \frac{\mathbf{V}_t[j] - Z_t}{s_t} \right\rfloor, 0, 2^b - 1 \right),$$

where:

$$Z_t = \min(\mathbf{V}_t[:]), s_t = \frac{\max(\mathbf{V}_t[:]) - \min(\mathbf{V}_t[:])}{2^b - 1}.$$

Here, the colon denotes iteration over all dimensions, following Python indexing syntax. Z_t is the zero-point, and s_t is the scaling factor. The function $\text{Clamp}(x, y, z)$ restricts the value of x to integers within the range $[y, z]$.

Outliers in key vectors (both pre-RoPE and post-RoPE) make per-token quantization challenging, as

we discussed earlier and illustrated in Figure 1(a). To address this, previous approaches (Liu et al., 2025; Hooper et al., 2024) quantize key vectors channel-wise. For example, for an arbitrary dimension i , a quantized pre-RoPE key vector $Q(\mathbf{K}_t)$ is given by:

$$Q(\mathbf{K}_t[j]) = \text{Clamp} \left(\left\lfloor \frac{\mathbf{K}_t[j] - Z_j}{s_j} \right\rfloor, 0, 2^b - 1 \right),$$

where the zero-point and scaling factor alternate as:

$$Z_j = \min(\mathbf{K}_{[:,j]}),$$

$$s_j = \frac{\max(\mathbf{K}_{[:,j]}) - \min(\mathbf{K}_{[:,j]})}{2^b - 1}.$$

Here, the colon in the subscript denotes iteration over all token positions.

Another challenge in quantizing key vectors is deciding whether to apply quantization before or after the RoPE. Quantizing the key vectors after applying RoPE faces a more complex outlier distribution, requiring tokens to be grouped for individual quantization, which adds additional overhead (Hooper et al., 2024). In contrast, outliers in pre-RoPE key vectors are more structured, but quantization in this case necessitates dequantization after retrieving keys from the cache and applying RoPE, which also introduces computational overhead. Addressing this dilemma is the central focus of this paper.

3 Method

We begin by presenting the key findings of outlier patterns in the key vectors (Section 3.1). These insights form the foundation for our novel and efficient quantization approach, PolarQuant (Section 3.2).

3.1 Motivation

As discussed earlier, outliers in key vectors pose a dilemma for researchers due to the overhead introduced by both pre-RoPE and post-RoPE channel-wise quantization. Our solution to this challenge arises from a key observation:

When mapping a paired dimension with outliers to polar coordinates, the outlier elements naturally form well-structured circular patterns, which simplify quantization.

Recall that in key vectors, elements in certain dimensions are jointly rotated by the same rotary sub-matrix \mathbf{r}_{n,ϕ_i} . Our analysis shows that the most

prominent outliers (highlighted in colors in Figure 1(a)) tend to occur in one of these dimension pairs.²

Because items in such paired dimensions are treated as two-dimensional vectors and rotated jointly, we are motivated to analyze these outliers in a two-dimensional plane. Figure 1(b) maps the paired dimensions from Figure 1(a) onto a 2D Cartesian coordinate system, where the x-axis represents the first dimension and the y-axis represents the second. Despite large variations in individual x and y values (which would indicate outliers in isolation), the mapped vectors form a well-structured pattern. In other words, when transformed into polar coordinates, the outliers are characterized by a smoothly distributed radial coordinate r and a polar angle θ . This structure significantly alleviates the quantization challenges faced by key caches.

3.2 PolarQuant: Polar-Coordinate-Based Quantization of Post-RoPE Key Vectors

Building on these insights, we propose a novel polar-coordinate-based quantization method, PolarQuant, designed for post-RoPE key vectors, which eliminates the need for token grouping. Because the advantages of using a polar-coordinate perspective to handle outliers were discussed in the previous subsection, here we focus on the implementation details.

For a 2D subvector $[\tilde{\mathbf{K}}_t[2j], \tilde{\mathbf{K}}_t[2j+1]]$ in a post-RoPE key vector at position t , where $0 \leq j < d/2$, we interpret $\tilde{\mathbf{K}}_t[2j]$ and $\tilde{\mathbf{K}}_t[2j+1]$ as Cartesian coordinates in the xy -plane. This 2D vector is then converted to polar coordinates, where the radius $r_t[j]$ is given by:

$$r_t[j] = \sqrt{\tilde{\mathbf{K}}_t[2j]^2 + \tilde{\mathbf{K}}_t[2j+1]^2},$$

and the polar angle is:

$$\theta_t[j] = \text{atan2}(\tilde{\mathbf{K}}_t[2j+1], \tilde{\mathbf{K}}_t[2j]) + \pi,$$

where $\text{atan2}(y, x)$ returns the angle between the positive x-axis and the point (x, y) , with a range of $(-\pi, \pi)$.

²For efficiency, the rotary matrix is typically applied in an element-wise multiplication manner (Su et al., 2023). To simplify implementation, dimensions i and $i + d/2$ are often rotated together, rather than i and $i + 1$. This results in non-adjacent outliers in Figure 1(a), but it does not affect our analysis, which is based on the matrix multiplication formulation (Eq. 1).

We quantize r_t and θ_t asymmetrically, using n -bit and m -bit precisions, respectively:

$$Q(r_t[j]) = \text{Clamp} \left(\left\lfloor \frac{r_t[j]}{s_j} \right\rfloor, 0, 2^n - 1 \right),$$

$$Q(\theta_t[j]) = \left\lfloor \frac{2^{m-1}\theta_t[j]}{\pi} \right\rfloor \bmod 2^m,$$

where:

$$s_j = \frac{\max(r_{[:j]})}{2^n - 1}.$$

Note that r_t does not have a quantization zero point because r_t is always greater than or equal to 0.

Intuitively, PolarQuant divides the two-dimensional plane into 2^{n+m} regions, spanned by 2^n radii and 2^m polar angles. A 2D sub-vector of the key vector is then represented by the region it locates at.

3.3 Efficient Decoding with PolarQuant

In this section, we introduce how PolarQuant performs decoding, with a particular focus on the query-key inner product step based on a quantized key cache. We highlight how it accelerates the decoding process.

Let us first review the dequantization process in traditional quantization methods. During decoding, the cached key vectors must be dequantized before performing the inner product with the current query token at position t . The dequantization process is formalized as follows, where \mathbf{K}'_t represents the dequantized key in floating-point precision. For each dimension $0 \leq j < d$, we have:

$$\mathbf{K}'_t[j] = Q(\mathbf{K}_t[j]) \cdot s_j + Z_j,$$

This dequantization introduces additional computational overhead. The inner product is then computed as $\mathbf{Q}_t \cdot \mathbf{K}'_{[:]}^\top$.

We argue that this overhead is redundant. At any dimension j , the dequantized outcomes belong to a finite set of size 2^b , where b is the quantization precision. This set depends entirely on the precision, and is unaffected by the shape or values of the quantized key. When the cache size far exceeds 2^b , it is more efficient to pre-compute and pick values from a lookup table, where the dequantized results have been stored. This is the key insight behind how PolarQuant accelerates multiplication.

Specifically, in PolarQuant, the lookup table is constructed by mapping quantized polar coordinates to Cartesian coordinates. The x - and y -axis values are then treated as separate elements in

the key vector’s specific dimensions. For a quantized representation $(Q(r_t[j]), Q(\theta_t[j]))$, the corresponding Cartesian coordinates in the key vector at dimensions $2j$ and $2j + 1$ are calculated as:

$$\begin{bmatrix} \tilde{\mathbf{K}}_t[2j] \\ \tilde{\mathbf{K}}_t[2j + 1] \end{bmatrix}^\top = \begin{bmatrix} \cos \left(\frac{\pi Q(\theta_t[j])}{2^{m-1}} \right) \cdot (Q(r_t[j]) \cdot s_j) \\ \sin \left(\frac{\pi Q(\theta_t[j])}{2^{m-1}} \right) \cdot (Q(r_t[j]) \cdot s_j) \end{bmatrix}^\top$$

Here, the sub-vector $[\tilde{\mathbf{K}}_t[2j], \tilde{\mathbf{K}}_t[2j + 1]]$ represents a state in the lookup table, which contains $\frac{d}{2} \times 2^m$ states in total (where $\frac{d}{2}$ is the number of sub-vectors in a key vector of dimension d , and 2^m is the number of quantized polar angle states). When computing the query-key inner product for the dimensions $2j$ and $2j + 1$, the result is:

$$\mathbf{IP}_{2j,2j+1} = \mathbf{Q}_t[2j] \cdot \tilde{\mathbf{K}}_t[2j] + \mathbf{Q}_t[2j+1] \cdot \tilde{\mathbf{K}}_t[2j+1],$$

and the final inner product is the sum:

$$\sum_{0 \leq j < \frac{d}{2}} \mathbf{IP}_{2j,2j+1}.$$

Previous methods cannot take advantage of this acceleration approach for several reasons. For methods based on pre-RoPE keys, dequantizing the key cache and performing multiplication with the RoPE matrix introduces pronounced overhead. In contrast, methods that focus on post-RoPE keys divide tokens into T/g groups, with each group having g tokens, and perform channel-wise quantization on the keys within each group. When g is small, it cannot exceed 2^b by much, leading to no efficiency gain, and possibly even slower inference. However, when g is large, inference performance is compromised.

4 Experiments

We compare PolarQuant with competitive key-value quantization algorithms. Since PolarQuant focuses on quantizing the key states, we first retain the value states in full precision (with fp16 as the default) to isolate and highlight the effectiveness of the quantized key cache (Section 4.1). Unless stated otherwise, the value states are kept in full precision throughout the following discussions.

4.1 Experiments on Key Quantization

We perform extensive experiments by quantizing various models and evaluating them across different tasks to demonstrate the effectiveness of PolarQuant.

Table 1: Evaluating quantization methods in long-text scenarios. We present experimental results from a series of advanced LLMs across a wide range of tasks in the LongBench benchmark. Actual bit widths for each method are estimated based on a context length of 12.2K tokens, which is the average input length of tokens on the LongBench.

Method	Actual Bit	Single Doc. QA			Multi Doc. QA			Summarization			Few-shot Learning			Avg.
		NtrvQA	Qasper	MF-en	2Wiki	Hotpot	Musique	GovRep	QMSum	MNews	TREC	TriviQA	SamSum	
<i>Llama-2-7B-Chat (4K)</i>														
fp16 Baseline	16	19.36	21.82	36.90	29.59	27.50	8.05	26.83	20.73	26.39	64.50	83.31	41.56	33.88
KVQuant-4bit-1%	4.32	18.88	17.60	32.98	30.79	24.74	8.40	25.64	20.67	25.96	64.50	83.61	41.29	32.92
KIVI-4-gs32-rs128	5.08	18.75	21.44	36.30	30.58	27.21	7.55	26.76	20.92	26.19	64.50	82.90	41.47	33.71
PolarQuant-m4n4	4.16	18.55	21.03	36.38	30.88	27.01	7.54	27.30	20.67	26.02	64.50	83.67	41.47	33.75
<i>Mistral-7B-Instruct-v0.2 (32K)</i>														
fp16 Baseline	16	26.73	33.01	49.34	27.35	43.02	18.78	32.81	24.15	27.09	68.50	86.48	41.12	39.87
KIVI-4-gs32-rs128	5.08	26.68	32.38	49.46	27.59	42.91	18.81	32.99	24.40	27.17	68.50	86.41	41.04	39.86
PolarQuant-m4n4	4.16	27.43	32.58	49.54	26.61	42.55	18.65	32.52	24.00	27.09	68.50	86.64	41.78	39.82
<i>Llama-3.1-8B-Instruct (128K)</i>														
fp16 Baseline	16	31.63	46.58	56.89	48.96	58.10	31.57	34.44	25.23	26.99	74.00	92.64	43.22	47.52
KIVI-4-gs32-rs128	5.08	30.97	46.43	56.66	49.13	58.02	31.46	34.52	25.36	27.29	74.00	92.46	43.57	47.49
PolarQuant-m4n4	4.16	32.50	46.16	56.73	48.97	57.91	31.67	34.04	25.47	26.76	74.00	92.86	43.07	47.51

Models We evaluate PolarQuant on a diverse set of advanced LLMs, including Llama-2-7B-Chat (Touvron et al., 2023), Llama-3.1-8B-Instruct (Grattafiori et al., 2024), and Mistral-7B-Instruct-v0.2 (Jiang et al., 2023). These models span three distinct families and cover varying scales. Notably, Llama-2-7B-Chat uses a multi-head attention (MHA) architecture, while the others employ grouped query attention (GQA (Ainslie et al., 2023)). Additionally, the models differ in their effective context lengths, ranging from 4k for Llama-2-7B to 128k for Llama-3.1-8B.

Tasks In this study, we primarily evaluate the performance of PolarQuant in long-context scenarios. Specifically, we compared PolarQuant with other quantization methods on the LongBench dataset (Bai et al., 2023), which is a widely used multitask benchmark for long-context understanding. We also assess quantization methods with inputs of typical context length, using the MMLU (Hendrycks et al., 2021) and GSM8K (Cobbe et al., 2021). These two tasks are evaluated in a 5-shot in-context learning setup. For GSM8K, the ICL demonstrations are formulated as chain-of-thought prompts.

Quantization Precision In our main experiments on both long-context and typical-length contexts, we adopt 4-bit precision because previous studies have shown that this precision can achieve performance comparable to full precision across multiple benchmarks. Note that group-wise and channel-wise quantization increase the number of quantization parameters, so the equivalent quantization bits

are larger than 4 in practice. In these 4-bit precision experiments, we report the actual quantization bits for all methods.

Although lower-bit quantization inevitably impairs performance, we explore the performance of PolarQuant under a lower-bit quantization setup, which is discussed in Section 4.2.

Kernel Implementation We implement the efficient decoding algorithm outlined in Section 3.3 as a fused Triton (Tillet et al., 2019) kernel, significantly reducing the number of floating-point operations required for query-key multiplication. This optimization follows the same principles as other efficient attention implementations, such as FlashAttention (Dao et al., 2022), which improves the General Matrix-Vector Product by partitioning the input into blocks and performing multiplication within each block. This block-based approach minimizes I/O operations through multiple passes, thereby accelerating the attention calculation. Additionally, by fusing the lookup operation with matrix multiplication in each block, PolarQuant ensures compatibility with FlashAttention, the widely used efficient attention implementation in advanced LLMs. A detailed analysis is provided in the ‘‘Efficiency Comparison’’ paragraph.

Results Table 1 show the results of PolarQuant on subtasks of LongBench. We exclude the KVQuant results for Mistral-7B-Instruct-v0.2 and Llama-3.1-8B-Instruct, as the KVQuant implementation is incompatible with the GQA setting. For KIVI, we use the default configuration with a group size of 32 and a residual length of 128.

Table 2: Performance comparisons between different cache quantization methods on MMLU and GSM8K, showing that our method remains competitive with the baselines on short contexts.

Model	Method	MMLU					GSM8k
		Humanities	Social Science	STEM	Other	Avg.	
<i>Llama-2-7b-Chat</i>	fp16 Baseline	38.46	56.54	35.19	58.49	47.17	24.79
	KIVI-4-gs32-rs128	38.53	55.39	35.45	59.26	47.16	23.96
	KVQuant-4bit-1%	38.85	57.52	34.39	57.52	47.07	22.67
	PolarQuant-m4n4	38.46	56.05	34.92	57.60	46.75	23.20
<i>Mistral-7B-Instruct-v0.2</i>	fp16 Baseline	48.57	68.46	45.50	68.45	57.75	39.42
	KIVI-4-gs32-rs128	48.17	68.46	45.50	68.45	57.64	39.42
	PolarQuant-m4n4	47.85	68.79	46.30	68.84	57.95	40.56
<i>Llama-3.1-8B-Instruct</i>	fp16 Baseline	53.98	78.76	55.82	73.95	65.63	78.47
	KIVI-4-gs32-rs128	53.91	78.76	56.08	73.95	65.68	79.00
	PolarQuant-m4n4	54.17	78.92	55.56	73.95	65.65	79.61

Table 3: The statistical results of the quantization parameters for PolarQuant. We take fp16 as the default full precision. The average bit width is estimated with $T = 12.2K$, $d = 128$, $g = 32$, and $s = 128$. Here, T represents the input sequence length, d is the dimension of the attention head, g is the group size, s is the residual length and α is the ratio of outliers saved in full precision. To simplify the formulation, we omit the batch size b and the number of attention heads n .

Method	Parameter Amount	Actual Bit
KIVI-4	$32Td / g + 16sd / 2$	$32 / g + 8sd / T$ 5.08
KVQuant	$32\alpha \cdot Td$	32α 4.32
PolarQuant	$16d / 2 + 16sd$	$8 / T + 16sd / T$ 4.16

For KVQuant, we adhere to the original 4-bit implementation as depicted in (Hooper et al., 2024). The experiments indicate that our method achieves comparable performance with existing 4-bit quantization baselines faced with challenging long context inputs. Moreover, the consistent performance preservation of PolarQuant across different models, scales, and attention architectures further emphasizes the robustness and generalizability of our approach in key states quantization.

Additionally, we evaluate PolarQuant’s performance with inputs of standard length. The results on MMLU and GSM8K are presented in Table 2. Similarly, we exclude the KVQuant results for Mistral and Llama-3.1 based on GQA architectures. We observe that our PolarQuant maintains competitive performance, with no significant decline in its parametric knowledge ability (MMLU) or in its planning and reasoning capacity for mathematical tasks (GSM8K). This indicates that our method effectively processes both long and short context

Table 4: Tested on an NVIDIA A800-SXM4-80GB GPU, PolarQuant reduces the average latency (in microseconds) of query-key multiplication compared to both fp16 PyTorch matrix multiplication and other baselines’ custom multiplication implementations. Here, query and key vectors are configured as $\mathbf{Q} \in \mathbb{R}^{1 \times 128}$ and $\mathbf{K} \in \mathbb{R}^{T \times 128}$, following the dimension settings of Llama-3.1, with the input length T varying.

Operation	$T = 4K$	$T = 8K$	$T = 32K$	$T = 128K$
FP16 Matmul	60.98	74.20	183.99	668.91
KIVI	97.08	133.92	427.24	1590.44
KVQuant	94.79	121.42	423.93	1834.58
PolarQuant	50.04	71.69	163.42	526.65

inputs, and the quantization operations introduced do not incur any notable loss in performance on knowledge-intensive and reasoning tasks.

Noteably, the actual quantization bit of PolarQuant is lower than baselines, indicating more efficient quantization, which we discuss in next paragraph, along with the practical query-key multiplication speed comparison.

Efficiency Comparison We discuss the quantization parameters required by each method and compare their practical running speeds, respectively.

(1) *Quantization Parameters Analysis.* We analyze the quantization parameter costs (e.g., the parameter amount of zeropoints and scales) of various quantization methods. Table 3 reports the average bit width estimated using LongBench, as it provides a more accurate reflection of the actual bit usage of the baseline methods in a long-context scenario.

In group-wise quantization methods such as KIVI, the fine-grained group partition introduces

Table 5: We report experimental results for PolarQuant-m4n2 on subtasks of the LongBench benchmark. We take Llama-3.1-8B-Instruct as backbone, with a quantization configuration of group size 64 and residual length 64. We compare PolarQuant-m4n2 with the 2-bit KIVI method, which uses a group size of 32 and a residual length of 128.

Method	Actual Bit	Single Doc. QA			Multi Doc. QA			Few-shot Learning		
		NtrvQA	Qasper	MF-en	2Wiki	Hotpot	Musique	TREC	TriviQA	Avg.
FP16 Baseline	16	31.63	46.58	56.89	48.96	58.10	31.57	74.00	92.64	55.05
KIVI-2-gs32-rs128	3.08	31.80	45.28	56.74	49.80	57.60	31.18	73.50	92.56	54.80
PolarQuant-m4n2	3.29	31.59	45.77	55.85	49.62	58.15	30.98	74.00	92.76	54.84

additional quantization overhead. For each group in KIVI, both the zero-point and the scale individually require 16 bits to store. For each channel in a single head, there are T/g groups, so the total quantization parameters is $2 \times 16 \times T \times d/g$, where d represents the number of channels (i.e., the dimension of the attention head). Consequently, the total number of parameters for a single head can reach up to $32Td/g$, resulting in a memory growth of the order $O(T)$.

PolarQuant has lower quantization costs for three reasons:

(i) PolarQuant does not need to group tokens before quantization, thus eliminating the cost of group-wise overhead.

(ii) The radius r only has $d/2$ channels to quantize.

(iii) The radius r is non-negative. We can always take zero as the zero point, so there are no zero points to store.

Note that KIVI retains a residual length s of locally relevant key states in full precision since this is crucial for challenging tasks such as reasoning (Liu et al., 2025). The window size is expected to be $s/2$, which is significantly smaller than the long context length T . Following KIVI, PolarQuant also retains a residual length of key states in full precision. This portion of the parameters occupies a smaller proportion of the overall quantization storage; therefore, this overhead is negligible in long-context scenario.

(2) *Query-Key Product Latency.* We evaluate the latency of query-key multiplication on an NVIDIA A800-SXM4-80GB GPU, demonstrating significant speedups with our kernel implementation compared to baseline methods.

Specifically, we record the wall-clock time of our custom query-key multiplication kernel. We test vector multiplication with a dimension of 128, a typical setting for 7B-parameter LLMs. The input sequence length T varies up to 128K tokens.

We benchmark runtime by summing across 1000 iterations of the multiplication operation. Our implementation is compared against PyTorch’s FP16 matrix multiplication and the batch matrix multiplications used in other key-cache quantization methods, such as KIVI and KVQuant. As shown in Table 4, PolarQuant consistently accelerates multiplication speed across different lengths, achieving up to a $1.27\times$ speedup over baseline methods, which can further enhance overall throughput.

4.2 Exploration under the 3-Bit Precision

In this section, we investigate the use of PolarQuant for low-bit key cache quantization. Specifically, we present a variant of PolarQuant, named PolarQuant-m4n2, in which a 4-bit integer quantizes the angles and a 2-bit integer quantizes the radii, yielding a quantization effect equivalent to a 3-bit approach. We compare PolarQuant-m4n2 with other low-bit quantization methods that share a similar number of quantization parameters. Experimental results, shown in Table 5, indicate that PolarQuant achieves competitive performance with other baseline methods at 3-bit. In future work, we will further explore low-bit quantization schemes based on PolarQuant.

5 Conclusion

In this paper, we view the outliers in the key cache of LLMs from a novel polar-coordinate-based perspective, which provides an efficient and effective solution, PolarQuant, to reduce the complexity and quantization costs in previous methods. PolarQuant well preserves downstream performance even in long-context scenarios, comparable to previous works under 4-bit precision while achieving superior efficiency. We hope the polar coordinate view can inspire the community to advance low-bit precision quantization techniques.

References

- Joshua Ainslie, James Lee-Thorp, Michiel de Jong, Yury Zemlyanskiy, Federico Lebron, and Sumit Sanghai. 2023. [GQA: Training generalized multi-query transformer models from multi-head checkpoints](#). In *Proceedings of the 2023 Conference on Empirical Methods in Natural Language Processing*, pages 4895–4901, Singapore. Association for Computational Linguistics.
- Dzmitry Bahdanau, Kyunghyun Cho, and Yoshua Bengio. 2016. [Neural machine translation by jointly learning to align and translate](#). *Preprint*, arXiv:1409.0473.
- Yushi Bai, Xin Lv, Jiajie Zhang, Hongchang Lyu, Jiankai Tang, Zhidian Huang, Zhengxiao Du, Xiao Liu, Aohan Zeng, Lei Hou, Yuxiao Dong, Jie Tang, and Juanzi Li. 2023. Longbench: A bilingual, multitask benchmark for long context understanding. *arXiv preprint arXiv:2308.14508*.
- Zefan Cai, Yichi Zhang, Bofei Gao, Yuliang Liu, Tianyu Liu, Keming Lu, Wayne Xiong, Yue Dong, Baobao Chang, Junjie Hu, and Wen Xiao. 2024. [Pyramidkv: Dynamic kv cache compression based on pyramidal information funneling](#). *Preprint*, arXiv:2406.02069.
- Karl Cobbe, Vineet Kosaraju, Mohammad Bavarian, Mark Chen, Heewoo Jun, Lukasz Kaiser, Matthias Plappert, Jerry Tworek, Jacob Hilton, Reiichiro Nakano, Christopher Hesse, and John Schulman. 2021. Training verifiers to solve math word problems. *arXiv preprint arXiv:2110.14168*.
- Tri Dao, Daniel Y. Fu, Stefano Ermon, Atri Rudra, and Christopher Ré. 2022. [Flashattention: Fast and memory-efficient exact attention with io-awareness](#). *Preprint*, arXiv:2205.14135.
- DeepSeek-AI, Aixin Liu, Bei Feng, Bin Wang, Bingxuan Wang, Bo Liu, Chenggang Zhao, Chengqi Deng, Chong Ruan, Damai Dai, Daya Guo, Dejian Yang, Deli Chen, Dongjie Ji, Erhang Li, Fangyun Lin, Fuli Luo, Guangbo Hao, Guanting Chen, Guowei Li, H. Zhang, Hanwei Xu, Hao Yang, Haowei Zhang, Honghui Ding, Huajian Xin, Huazuo Gao, Hui Li, Hui Qu, J. L. Cai, Jian Liang, Jianzhong Guo, Jiaqi Ni, Jiashi Li, Jin Chen, Jingyang Yuan, Junjie Qiu, Junxiao Song, Kai Dong, Kaige Gao, Kang Guan, Lean Wang, Lecong Zhang, Lei Xu, Leyi Xia, Liang Zhao, Liyue Zhang, Meng Li, Miaojun Wang, Mingchuan Zhang, Minghua Zhang, Minghui Tang, Mingming Li, Ning Tian, Panpan Huang, Peiyi Wang, Peng Zhang, Qihao Zhu, Qinyu Chen, Qishi Du, R. J. Chen, R. L. Jin, Ruiqi Ge, Ruizhe Pan, Runxin Xu, Ruyi Chen, S. S. Li, Shanghao Lu, Shangyan Zhou, Shanhuang Chen, Shaoqing Wu, Shengfeng Ye, Shirong Ma, Shiyu Wang, Shuang Zhou, Shuiping Yu, Shunfeng Zhou, Size Zheng, T. Wang, Tian Pei, Tian Yuan, Tianyu Sun, W. L. Xiao, Wangding Zeng, Wei An, Wen Liu, Wenfeng Liang, Wenjun Gao, Wentao Zhang, X. Q. Li, Xiangyue Jin, Xianzu Wang, Xiao Bi, Xiaodong Liu, Xiaohan Wang, Xiaojin Shen, Xiaokang Chen, Xiaosha Chen, Xiaotao Nie, Xiaowen Sun, Xiaoxiang Wang, Xin Liu, Xin Xie, Xingkai Yu, Xinnan Song, Xinyi Zhou, Xinyu Yang, Xuan Lu, Xuecheng Su, Y. Wu, Y. K. Li, Y. X. Wei, Y. X. Zhu, Yanhong Xu, Yanping Huang, Yao Li, Yao Zhao, Yaofeng Sun, Yaohui Li, Yaohui Wang, Yi Zheng, Yichao Zhang, Yiliang Xiong, Yilong Zhao, Ying He, Ying Tang, Yishi Piao, Yixin Dong, Yixuan Tan, Yiyuan Liu, Yongji Wang, Yongqiang Guo, Yuchen Zhu, Yuduan Wang, Yuheng Zou, Yukun Zha, Yunxian Ma, Yuting Yan, Yuxiang You, Yuxuan Liu, Z. Z. Ren, Zehui Ren, Zhangli Sha, Zhe Fu, Zhen Huang, Zhen Zhang, Zhenda Xie, Zhewen Hao, Zhihong Shao, Zhiniu Wen, Zhipeng Xu, Zhongyu Zhang, Zhuoshu Li, Zihan Wang, Zihui Gu, Zilin Li, and Ziwei Xie. 2024. [Deepseek-v2: A strong, economical, and efficient mixture-of-experts language model](#). *Preprint*, arXiv:2405.04434.
- Aaron Grattafiori, Abhimanyu Dubey, Abhinav Jauhri, Abhinav Pandey, Abhishek Kadian, Ahmad Al-Dahle, Aiesha Letman, Akhil Mathur, Alan Schelten, Alex Vaughan, Amy Yang, Angela Fan, Anirudh Goyal, Anthony Hartshorn, Aobo Yang, Archi Mitra, Archie Sravankumar, Artem Korenev, Arthur Hinsvark, Arun Rao, Aston Zhang, Aurelien Rodriguez, Austen Gregerson, Ava Spataru, Baptiste Roziere, Bethany Biron, Binh Tang, Bobbie Chern, Charlotte Caucheteux, Chaya Nayak, Chloe Bi, Chris Marra, Chris McConnell, Christian Keller, Christophe Touret, Chunyang Wu, Corinne Wong, Cristian Canton Ferrer, Cyrus Nikolaidis, Damien Alonsoius, Daniel Song, Danielle Pintz, Danny Livshits, Danny Wyatt, David Esiobu, Dhruv Choudhary, Dhruv Mahajan, Diego Garcia-Olano, Diego Perino, Dieuwke Hupkes, Egor Lakomkin, Ehab AlBadawy, Elina Lobanova, Emily Dinan, Eric Michael Smith, Filip Radenovic, Francisco Guzmán, Frank Zhang, Gabriel Synnaeve, Gabrielle Lee, Georgia Lewis Anderson, Govind Thattai, Graeme Nail, Gregoire Mialon, Guan Pang, Guillem Cucurell, Hailey Nguyen, Hannah Korevaar, Hu Xu, Hugo Touvron, Iliyan Zarov, Imanol Arrieta Ibarra, Isabel Kloumann, Ishan Misra, Ivan Evtimov, Jack Zhang, Jade Copet, Jaewon Lee, Jan Geffert, Jana Vranes, Jason Park, Jay Mahadeokar, Jeet Shah, Jelmer van der Linde, Jennifer Billock, Jenny Hong, Jenya Lee, Jeremy Fu, Jianfeng Chi, Jianyu Huang, Jiawen Liu, Jie Wang, Jiecao Yu, Joanna Bitton, Joe Spisak, Jongsoo Park, Joseph Rocca, Joshua Johnstun, Joshua Saxe, Junteng Jia, Kalyan Vasuden Alwala, Karthik Prasad, Kartikeya Upasani, Kate Plawiak, Ke Li, Kenneth Heafield, Kevin Stone, Khalid El-Arini, Krithika Iyer, Lshith Malik, Kuenley Chiu, Kunal Bhalla, Kushal Lakhotia, Lauren Rantala-Yearly, Laurens van der Maaten, Lawrence Chen, Liang Tan, Liz Jenkins, Louis Martin, Lovish Madaan, Lubo Malo, Lukas Blecher, Lukas Landzaat, Luke de Oliveira, Madeline Muzzi, Mahesh Pasupuleti, Mannat Singh, Manohar Paluri, Marcin Kardas, Maria Tsimpoukelli, Mathew Oldham, Mathieu Rita, Maya Pavlova, Melanie Kam-badur, Mike Lewis, Min Si, Mitesh Kumar Singh, Mona Hassan, Naman Goyal, Narjes Torabi, Nikolay Bashlykov, Nikolay Bogoychev, Niladri Chatterji,

Ning Zhang, Olivier Duchenne, Onur Çelebi, Patrick Alrassy, Pengchuan Zhang, Pengwei Li, Petar Vasic, Peter Weng, Prajjwal Bhargava, Pratik Dubal, Praveen Krishnan, Punit Singh Koura, Puxin Xu, Qing He, Qingxiao Dong, Ragavan Srinivasan, Raj Ganapathy, Ramon Calderer, Ricardo Silveira Cabral, Robert Stojnic, Roberta Raileanu, Rohan Maheswari, Rohit Girdhar, Rohit Patel, Romain Sauvestre, Ronnie Polidoro, Roshan Sumbaly, Ross Taylor, Ruan Silva, Rui Hou, Rui Wang, Saghar Hosseini, Sahana Chennabasappa, Sanjay Singh, Sean Bell, Seohyun Sonia Kim, Sergey Edunov, Shaoliang Nie, Sharan Narang, Sharath Rapparthi, Sheng Shen, Shengye Wan, Shruti Bhosale, Shun Zhang, Simon Vandenhende, Soumya Batra, Spencer Whitman, Sten Sootla, Stephane Collot, Suchin Gururangan, Sydney Borodinsky, Tamar Herman, Tara Fowler, Tarek Sheasha, Thomas Georgiou, Thomas Scialom, Tobias Speckbacher, Todor Mihaylov, Tong Xiao, Ujjwal Karn, Vedanuj Goswami, Vibhor Gupta, Vignesh Ramanathan, Viktor Kerkez, Vincent Gouget, Virginie Do, Vish Vogeti, Vítor Albiero, Vladan Petrovic, Weiwei Chu, Wenhan Xiong, Wenyin Fu, Whitney Meers, Xavier Martinet, Xiaodong Wang, Xiaofang Wang, Xiaoqing Ellen Tan, Xide Xia, Xinfeng Xie, Xuchao Jia, Xuewei Wang, Yaelle Goldschlag, Yashesh Gaur, Yasmine Babaei, Yi Wen, Yiwen Song, Yuchen Zhang, Yue Li, Yuning Mao, Zacharie Delpierre Coudert, Zheng Yan, Zhengxing Chen, Zoe Papakipos, Aaditya Singh, Aayushi Srivastava, Abha Jain, Adam Kelsey, Adam Shajnfeld, Adithya Gangidi, Adolfo Victoria, Ahuva Goldstand, Ajay Menon, Ajay Sharma, Alex Boesenberg, Alexei Baevski, Allie Feinstein, Amanda Kallet, Amit Sangani, Amos Teo, Anam Yunus, Andrei Lupu, Andres Alvarado, Andrew Caples, Andrew Gu, Andrew Ho, Andrew Poulton, Andrew Ryan, Ankit Ramchandani, Annie Dong, Annie Franco, Anuj Goyal, Aparajita Saraf, Arkabandhu Chowdhury, Ashley Gabriel, Ashwin Bharambe, Assaf Eisenman, Azadeh Yazdan, Beau James, Ben Maurer, Benjamin Leonhardi, Bernie Huang, Beth Loyd, Beto De Paola, Bhargavi Paranjape, Bing Liu, Bo Wu, Boyu Ni, Braden Hancock, Bram Wasti, Brandon Spence, Brani Stojkovic, Brian Gamido, Britt Montalvo, Carl Parker, Carly Burton, Catalina Mejia, Ce Liu, Changan Wang, Changkyu Kim, Chao Zhou, Chester Hu, Ching-Hsiang Chu, Chris Cai, Chris Tindal, Christoph Feichtenhofer, Cynthia Gao, Damon Civin, Dana Beaty, Daniel Kreymer, Daniel Li, David Adkins, David Xu, Davide Testuggine, Delia David, Devi Parikh, Diana Liskovich, Didem Foss, Dingkan Wang, Duc Le, Dustin Holland, Edward Dowling, Eissa Jamil, Elaine Montgomery, Eleonora Presani, Emily Hahn, Emily Wood, Eric-Tuan Le, Erik Brinkman, Esteban Arcaute, Evan Dunbar, Evan Smothers, Fei Sun, Felix Kreuk, Feng Tian, Filippos Kokkinos, Firat Ozgenel, Francesco Caggioni, Frank Kanayet, Frank Seide, Gabriela Medina Florez, Gabriella Schwarz, Gada Badeer, Georgia Swee, Gil Halpern, Grant Herman, Grigory Sizov, Guangyi, Zhang, Guna Lakshminarayanan, Hakan Inan, Hamid Shojanazeri, Han Zou, Hannah Wang, Hanwen Zha, Haroun Habeeb, Harrison Rudolph, Helen Suk, Henry As-

pegren, Hunter Goldman, Hongyuan Zhan, Ibrahim Damlaj, Igor Molybog, Igor Tufanov, Ilias Leontiadis, Irina-Elena Veliche, Itai Gat, Jake Weissman, James Geboski, James Kohli, Janice Lam, Japhet Asher, Jean-Baptiste Gaya, Jeff Marcus, Jeff Tang, Jennifer Chan, Jenny Zhen, Jeremy Reizenstein, Jeremy Teboul, Jessica Zhong, Jian Jin, Jingyi Yang, Joe Cummings, Jon Carvill, Jon Shepard, Jonathan McPhie, Jonathan Torres, Josh Ginsburg, Junjie Wang, Kai Wu, Kam Hou U, Karan Saxena, Kartikay Khandelwal, Katayoun Zand, Kathy Matosich, Kaushik Veeraraghavan, Kelly Michelena, Keqian Li, Kiran Jagadeesh, Kun Huang, Kunal Chawla, Kyle Huang, Lailin Chen, Lakshya Garg, Lavender A, Leandro Silva, Lee Bell, Lei Zhang, Liangpeng Guo, Licheng Yu, Liron Moshkovich, Luca Wehrstedt, Madian Khabsa, Manav Avalani, Manish Bhatt, Martynas Mankus, Matan Hasson, Matthew Lennie, Matthias Reso, Maxim Groshev, Maxim Naumov, Maya Lathi, Meghan Keneally, Miao Liu, Michael L. Seltzer, Michal Valko, Michelle Restrepo, Mihir Patel, Mik Vyatskov, Mikayel Samvelyan, Mike Clark, Mike Macey, Mike Wang, Miquel Jubert Hermoso, Mo Metanat, Mohammad Rastegari, Munish Bansal, Nandhini Santhanam, Natascha Parks, Natasha White, Navyata Bawa, Nayan Singhal, Nick Egebo, Nicolas Usunier, Nikhil Mehta, Nikolay Pavlovich Laptev, Ning Dong, Norman Cheng, Oleg Chernoguz, Olivia Hart, Omkar Salpekar, Ozlem Kalinli, Parkin Kent, Parth Parekh, Paul Saab, Pavan Balaji, Pedro Rittner, Philip Bontrager, Pierre Roux, Piotr Dollar, Polina Zvyagina, Prashant Ratanchandani, Pritish Yuvraj, Qian Liang, Rachad Alao, Rachel Rodriguez, Rafi Ayub, Raghotham Murthy, Raghu Nayani, Rahul Mitra, Rangaprabhu Parthasarathy, Raymond Li, Rebekkah Hogan, Robin Battey, Rocky Wang, Russ Howes, Ruty Rinott, Sachin Mehta, Sachin Siby, Sai Jayesh Bondu, Samyak Datta, Sara Chugh, Sara Hunt, Sargun Dhillon, Sasha Sidorov, Satadru Pan, Saurabh Mahajan, Saurabh Verma, Seiji Yamamoto, Sharadh Ramaswamy, Shaun Lindsay, Shaun Lindsay, Sheng Feng, Shenghao Lin, Shengxin Cindy Zha, Shishir Patil, Shiva Shankar, Shuqiang Zhang, Shuqiang Zhang, Sinong Wang, Sneha Agarwal, Soji Sajuyigbe, Soumith Chintala, Stephanie Max, Stephen Chen, Steve Kehoe, Steve Satterfield, Sudarshan Govindaprasad, Sumit Gupta, Summer Deng, Sungmin Cho, Sunny Virk, Suraj Subramanian, Sy Choudhury, Sydney Goldman, Tal Remez, Tamar Glaser, Tamara Best, Thilo Koehler, Thomas Robinson, Tianhe Li, Tianjun Zhang, Tim Matthews, Timothy Chou, Tzook Shaked, Varun Vontimitta, Victoria Ajayi, Victoria Montanez, Vijai Mohan, Vinay Satish Kumar, Vishal Mangla, Vlad Ionescu, Vlad Poenaru, Vlad Tiberiu Mihailescu, Vladimir Ivanov, Wei Li, Wenchen Wang, Wenwen Jiang, Wes Bouaziz, Will Constable, Xiaocheng Tang, Xiaojian Wu, Xiaolan Wang, Xilun Wu, Xinbo Gao, Yaniv Kleinman, Yanjun Chen, Ye Hu, Ye Jia, Ye Qi, Yenda Li, Yilin Zhang, Ying Zhang, Yossi Adi, Youngjin Nam, Yu, Wang, Yu Zhao, Yuchen Hao, Yundi Qian, Yunlu Li, Yuzi He, Zach Rait, Zachary DeVito, Zef Rosnbrick, Zhaoduo Wen, Zhenyu Yang, Zhiwei Zhao, and Zhiyu Ma. 2024. [The llama 3 herd](#)

- of models. *Preprint*, arXiv:2407.21783.
- Dan Hendrycks, Collin Burns, Steven Basart, Andy Zou, Mantas Mazeika, Dawn Song, and Jacob Steinhardt. 2021. [Measuring massive multitask language understanding](#). *Preprint*, arXiv:2009.03300.
- Coleman Hooper, Sehoon Kim, Hiva Mohammadzadeh, Michael W. Mahoney, Yakun Sophia Shao, Kurt Keutzer, and Amir Gholami. 2024. [Kvquant: Towards 10 million context length llm inference with kv cache quantization](#). *Preprint*, arXiv:2401.18079.
- Albert Q. Jiang, Alexandre Sablayrolles, Arthur Mensch, Chris Bamford, Devendra Singh Chaplot, Diego de las Casas, Florian Bressand, Gianna Lengyel, Guillaume Lample, Lucile Saulnier, L elio Renard Lavaud, Marie-Anne Lachaux, Pierre Stock, Teven Le Scao, Thibaut Lavril, Thomas Wang, Timoth e Lacroix, and William El Sayed. 2023. [Mistral 7b](#). *Preprint*, arXiv:2310.06825.
- Hao Kang, Qingru Zhang, Souvik Kundu, Geonhwa Jeong, Zaoxing Liu, Tushar Krishna, and Tuo Zhao. 2024. [Gear: An efficient kv cache compression recipe for near-lossless generative inference of llm](#). *Preprint*, arXiv:2403.05527.
- Yuhong Li, Yingbing Huang, Bowen Yang, Bharat Venkitesh, Acyr Locatelli, Hanchen Ye, Tianle Cai, Patrick Lewis, and Deming Chen. 2024. [Snapkv: Llm knows what you are looking for before generation](#). *arXiv preprint arXiv:2404.14469*.
- Nelson F. Liu, Kevin Lin, John Hewitt, Ashwin Paranjape, Michele Bevilacqua, Fabio Petroni, and Percy Liang. 2024. [Lost in the middle: How language models use long contexts](#). *Transactions of the Association for Computational Linguistics*, 12:157–173.
- Zirui Liu, Jiayi Yuan, Hongye Jin, Shaochen (Henry) Zhong, Zhaozhuo Xu, Vladimir Braverman, Beidi Chen, and Xia Hu. 2025. [Kivi: a tuning-free asymmetric 2bit quantization for kv cache](#). In *Proceedings of the 41st International Conference on Machine Learning, ICML’24*. JMLR.org.
- OpenAI. 2024. [Learning to reason with llms](https://openai.com/index/learning-to-reason-with-llms/). <https://openai.com/index/learning-to-reason-with-llms/>. [Accessed 19-09-2024].
- Jianlin Su, Yu Lu, Shengfeng Pan, Ahmed Murtadha, Bo Wen, and Yunfeng Liu. 2023. [Roformer: Enhanced transformer with rotary position embedding](#). *Preprint*, arXiv:2104.09864.
- Philippe Tillet, H. T. Kung, and David Cox. 2019. [Triton: an intermediate language and compiler for tiled neural network computations](#).
- Hugo Touvron, Louis Martin, Kevin Stone, Peter Albert, Amjad Almahairi, Yasmine Babaei, Nikolay Bashlykov, Soumya Batra, Prajjwal Bhargava, Shruti Bhosale, Dan Bikel, Lukas Blecher, Cristian Canton Ferrer, Moya Chen, Guillem Cucurull, David Esiobu, Jude Fernandes, Jeremy Fu, Wenyin Fu, Brian Fuller, Cynthia Gao, Vedanuj Goswami, Naman Goyal, Anthony Hartshorn, Saghar Hosseini, Rui Hou, Hakan Inan, Marcin Kardas, Viktor Kerkez, Madian Khabsa, Isabel Kloumann, Artem Korenev, Punit Singh Koura, Marie-Anne Lachaux, Thibaut Lavril, Jenya Lee, Diana Liskovich, Yinghai Lu, Yuning Mao, Xavier Martinet, Todor Mihaylov, Pushkar Mishra, Igor Molybog, Yixin Nie, Andrew Poulton, Jeremy Reizenstein, Rashi Rungta, Kalyan Saladi, Alan Schelten, Ruan Silva, Eric Michael Smith, Ranjan Subramanian, Xiaoqing Ellen Tan, Binh Tang, Ross Taylor, Adina Williams, Jian Xiang Kuan, Puxin Xu, Zheng Yan, Iliyan Zarov, Yuchen Zhang, Angela Fan, Melanie Kambadur, Sharan Narang, Aurelien Rodriguez, Robert Stojnic, Sergey Edunov, and Thomas Scialom. 2023. [Llama 2: Open foundation and fine-tuned chat models](#). *Preprint*, arXiv:2307.09288.
- Ashish Vaswani, Noam Shazeer, Niki Parmar, Jakob Uszkoreit, Llion Jones, Aidan N Gomez, Łukasz Kaiser, and Illia Polosukhin. 2017. [Attention is all you need](#). In *Advances in Neural Information Processing Systems*, volume 30. Curran Associates, Inc.
- Zhenyu Zhang, Ying Sheng, Tianyi Zhou, Tianlong Chen, Lianmin Zheng, Ruisi Cai, Zhao Song, Yuan-dong Tian, Christopher R e, Clark Barrett, Zhangyang Wang, and Beidi Chen. 2023. [H2o: Heavy-hitter oracle for efficient generative inference of large language models](#). *Preprint*, arXiv:2306.14048.
- Yilong Zhao, Chien-Yu Lin, Kan Zhu, Zihao Ye, Lequn Chen, Size Zheng, Luis Ceze, Arvind Krishnamurthy, Tianqi Chen, and Baris Kasikci. 2024. [Atom: Low-bit quantization for efficient and accurate llm serving](#). In *Proceedings of Machine Learning and Systems*, volume 6, pages 196–209.